water

MDPI

Article

An Evaluation of Secondary Mineral Formation/Dissolution and Phase Separation Based on Mg Isotopic Fractionation: The Shallow-Water Hydrothermal System in Milos, Greece

Yi-Chi Chen [1,2], Chen-Feng You [2,*], Chuan-Hsiung Chung [2], Kuo-Fang Huang [3], Shein-Fu Wu [2,4], Eugenia Valsami-Jones [5] and Emmanuel Baltatzis [6]

1 Green Energy and Environment Research Laboratories, Industrial Technology Research Institute, Tainan 71101, Taiwan; itrib00341@itri.org.tw
2 Department of Earth Sciences, National Cheng Kung University, Tainan 70101, Taiwan; bear_chung@mail.ncku.edu.tw (C.-H.C.); sheinfuwu@ntu.edu.tw (S.-F.W.)
3 Institute of Earth Sciences, Academia Sinica, Taipei 11529, Taiwan; kfhuang@earth.sinica.edu.tw
4 Institute of Oceanography, National Taiwan University, No. 1, Section 4, Roosevelt Road, Da'an District, Taipei 106, Taiwan
5 School of Geography, Earth and Environmental Sciences, University of Birmingham, Birmingham B15 2TT, UK; e.valsamijones@bham.ac.uk
6 Department of Geology and Geo-Environment, National and Kapodistrian University of Athens, GR 157 84 Athens, Greece; baltatzis@geol.uoa.gr
* Correspondence: cfy20@mail.ncku.edu.tw

Abstract: This study investigates Mg isotopes (δ^{26}Mg) in vent fluids from Milos, Aegean Sea, to evaluate phase separation and secondary mineral formation. The δ^{26}Mg vary significantly in Milos, exceeding 0.66‰, allowing for the classification of the fluids into three sub-groups based on chemical characteristics: seawater-like, cave fluids, and submarine-brines. The seawater-like fluids exhibit large δ^{26}Mg variation, −0.64 to −1.18‰, and mostly follow a Rayleigh fractionation trend, with a fractionation factor $\alpha = 1.00020 \pm 0.00011$. The cave fluids are highly acidic, have low Cl, are vapor-rich, and display heavy δ^{26}Mg compositions (−0.52 to −0.63‰). The submarine-brines are characterized by high Cl, high non-volatile metals, and light δ^{26}Mg (−0.65 to −1.00‰). The latter two fluid types represent vapors and brines, respectively, which underwent phase separation at depth in Milos. These δ^{26}Mg values were combined with major/trace elements, as well as Li and B isotopes, to explore possible controlling mechanisms. We report for the first time a shallow submarine hydrothermal system that has a vapor component enriched in heavy δ^{26}Mg, but with no detectable isotopic changes in the brines. It is evident that δ^{26}Mg in vent fluids is unique for separating effects of water/rock interaction and secondary mineral and phase separation at shallow-water systems.

Keywords: Mg isotopes; hydrothermal vent fluids; water/rock interaction; Rayleigh fractionation; phase separation

check for updates

Academic Editors: Daniel D. Snow, Staša Borović and Josip Terzić

Received: 12 December 2024
Revised: 8 January 2025
Accepted: 26 January 2025
Published: 28 January 2025

Citation: Chen, Y.-C.; You, C.-F.; Chung, C.-H.; Huang, K.-F.; Wu, S.-F.; Valsami-Jones, E.; Baltatzis, E. An Evaluation of Secondary Mineral Formation/Dissolution and Phase Separation Based on Mg Isotopic Fractionation: The Shallow-Water Hydrothermal System in Milos, Greece. *Water* **2025**, *17*, 370. https://doi.org/10.3390/w17030370

Copyright: © 2025 by the authors. Licensee MDPI, Basel, Switzerland. This article is an open access article distributed under the terms and conditions of the Creative Commons Attribution (CC BY) license (https://creativecommons.org/licenses/by/4.0/).

1. Introduction

Hydrothermal systems are prevalent in tectonically active settings, including convergent margins, plate boundaries, and hot spots. They are commonly categorized by water depth into two groups: (1) deep-sea (water depth > 200 m) and (2) shallow-sea (water depth < 200 m) [1–3]. These systems are often discussed separately due to differences in biological community structure, geological setting, and physical or chemical conditions in the environment [4]. Over the past decade, the literature has mainly focused on deep

hydrothermal systems with high temperatures at mid-ocean ridges or various subduction zones [5]. Research on shallow hydrothermal systems is rather scarce. However, the latter are located in regions that are easier to access for sampling and can be studied with relatively low operational costs for extensive field surveys [6,7]. Milos Island, Greece, is well-known for its mineral wealth, especially clay deposits, as well as the island's shallow-water hydrothermal vent system, where water/rock interactions have dominated the geology and mineralogy of the island, producing an active hot water venting system and numerous secondary mineral deposits.

Magnesium (Mg) has three major stable isotopes, ^{24}Mg, ^{25}Mg, and ^{26}Mg, with relative abundance of 78.99, 10.00, and 11.01%, respectively [8]. The mass difference between ^{24}Mg and ^{26}Mg is rather large, >8%, making them powerful tracers for various geological processes [9]. Modern seawater shows a homogeneous Mg content (52.8 mmol/L, [10]) and δ^{26}Mg isotopic composition (-0.83 ± 0.09 ‰, [11]). Magnesium isotope fractionation occurs via two mechanisms. First, magmatic fractionation causes ~2.5‰ variation in silicate minerals due to differences in mineral structure and bond strength. Second, weathering in low-temperature environments results in ~6‰ variation, driven by the weathering of primary minerals and the formation of secondary minerals [9].

Most studies indicate that carbonate minerals, such as calcite and dolomite, contain significantly lighter δ^{26}Mg (-1.05~-4.85‰) compared to silicates (0.02~-1.09‰) [12,13]. However, it was found that compared to fresh mid-ocean ridge basalt (MORB), δ^{26}Mg values of the altered oceanic crust (AOC) are highly heterogeneous, ranging from -1.70 to 0.21‰, indicating significant Mg isotope fractionation during low-temperature alteration of the oceanic crust [13]. Several recent studies have shown that significant Mg isotopic fractionations occurred during crust alteration, where heavier Mg isotopes preferentially enter minerals at T > 90 °C (Figure S1) [13–19]. These studies conclude that δ^{26}Mg can be a sensitive water/rock interactions tracer of low-temperature alteration in hydrothermal systems [13,15,17]. Most of these experiments have removed the influence of exchangeable Mg in calculations, such as Vigier et al. [20] and Ryu et al. [15]. For example, (1) a fraction of the synthesized clay was saturated three times with NH_4Cl in order to remove all exchangeable Mg [20]; (2) powder was reacted with 10 mL of 1 M NH_4Ac for 6 h (pH = 7) using a Thermo Scientific Vari-Mix™ Test Tube Rocker. The mixture was centrifuged, and the supernatant was passed through a 0.45 µm polypropylene syringe filter, dried, and re-dissolved in 5% HNO_3. The residue was then reacted with 10 mL of 4 M HAc for 6 h (pH = 2) using a Thermo Scientific Vari-Mix™ Test Tube Rocker. The mixture was centrifuged, and the supernatant was passed through a 0.45 µm polypropylene syringe filter [15]. However, the amount of exchangeable Mg is relatively small compared to the total mineral content [18].

$$\alpha^{26/24}_{\text{solid}-\text{liquid}} \equiv \frac{^{26}\text{Mg}_{\text{solid}}/^{24}\text{Mg}_{\text{solid}}}{^{26}\text{Mg}_{\text{liquid}}/^{24}\text{Mg}_{\text{liquid}}} \quad (1)$$

$$\alpha^{26/24}_{\text{solid}-\text{liquid}} - 1 = \varepsilon^{26/24}_{\text{solid}-\text{liquid}} \quad (2)$$

where α is the fractionation factor and ε is the isotopic difference between the solids and liquids.

Previously, Li and B isotopes have been measured in Milos fluids collected in 2002/2003 to elucidate the fluid circulation in the Milos hydrothermal system [21–23]. Two types of seawater circulation modes have been identified: shallow circulation and deep circulation. The former occurs at depths approximately 0.5 km, with temperatures below 248 °C and the latter occurs at depths approximately 1–2 km, with temperatures exceeding 313 °C. The shallow circulation produces seawater-like fluids with partial re-

moval of Mg, rather high pH (pH = 5~7), and a wide range of $\delta^{11}B$ and $\delta^{7}Li$ values. The deep circulation undergoes phase separation, fractionating the fluids into vapor and brine phases [21,22]. Two factors may contribute to the co-existence of vapors and brine fluids in Milos: (1) its shallow depth, which allows fluids to reach high temperatures at relatively low pressures [24], and (2) high H_2O levels of vapor, CO_2, and H_2S resulting from the addition of magmatic activity-generated volatiles produced in this island arc setting [25]. The CO_2 addition could change the critical point of seawater to higher pressures and lower temperatures, as suggested by previous experimental studies [24,26].

This study aims to apply new magnesium (Mg) isotopic measurements, along with other available geochemical data, to identify possible sources and to evaluate water–rock interactions in the Milos hydrothermal system, with a particular focus on low-temperature alteration in shallow-depth circulation. We hypothesize that the fractionation of Mg isotopes is influenced by distinct mechanisms during water–rock interactions and phase separation, which can be characterized by isotopic measurements and geochemical modeling. To address these questions, we classified the Milos vent fluids into three categories: (1) seawater-like fluids; (2) vapor-enriched fluids; and (3) submarine-brine fluids. We used the Rayleigh fractionation model to explore the fractionation mechanisms of seawater-like hydrothermal fluids and further evaluated Mg isotopic fractionation in vapor-enriched and brine fluids through their chloride (Cl) concentrations. Previous studies on magnesium isotopes in hydrothermal fluids have been limited, particularly in shallow hydrothermal systems. This research provides novel insights into the processes governing Mg isotopic fractionation during water–rock interactions and phase separation. By integrating Mg isotopes with lithium (Li) and boron (B) isotopic data [21–23,27], our study contributes to a more comprehensive understanding of hydrothermal circulation and the geochemical evolution of the Milos system.

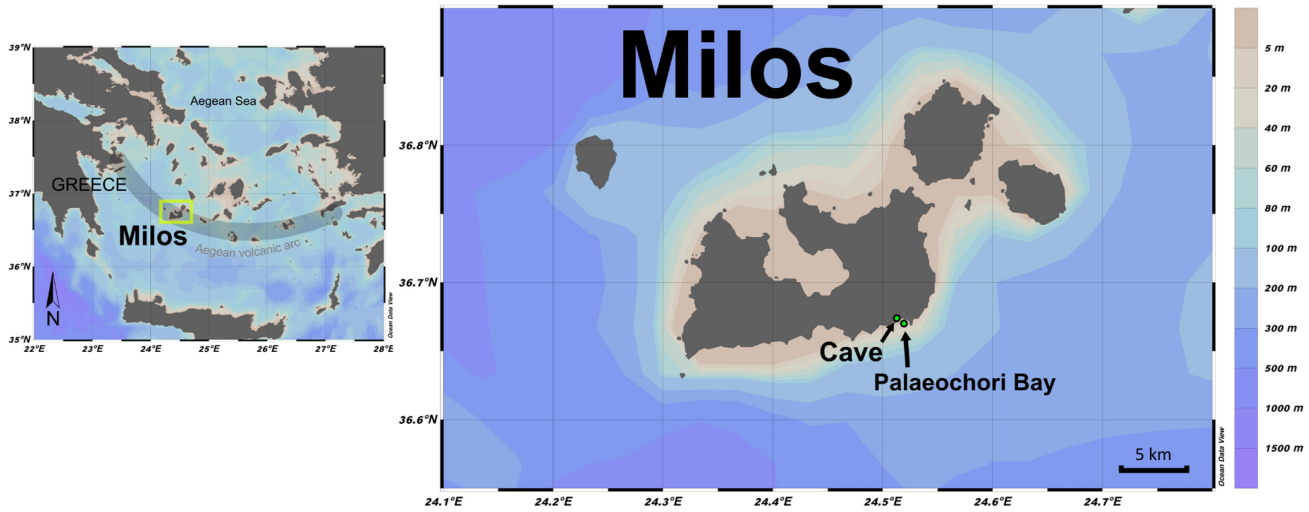
2. Materials and Methods

2.1. Geological Settings

The island of Milos is one of the islands forming a volcanic arc in the Aegean Sea, which is located between the African Plate and the Aegean Sea Plate in the Mediterranean Sea. The volcanic system in the south of Milos Island has lain dormant for the past 90,000 years; however, its residual heat continues to drive hydrothermal circulation in a number of locations around the island. Numerous locations off the south coast of the island exhibit submarine hydrothermal activity (see Figure 1). On land, hydrothermally active areas indicated by extreme rock weathering; representing between 1.7% and ~2% of the total mapped surface, ~3.4 km^2 [6,28–30].

Paleochori Bay, the most active hydrothermal area of the island, is located on the SE coast. This is where vent fluids studied in this work were collected. Andesite and dacite are the dominant volcanic rocks in this region [30,31]. Modern sediments, composed of 94% alumino-silicates, 0.02% carbonates, and 5% Fe-Mn oxides, have accumulated at the surface with a thickness of at least 5 m [32]. Compared with other submarine hydrothermal fields in Greece, Milos Island has the highest proportion of alumino-silicates but the lowest proportion of carbonates [32].

Due to its extensive hydrothermal activity, various minerals are formed in Milos, including natural metallic or non-metallic minerals [33]. It is the most mineralized island in Europe, evidenced by an extensive shallow hydrothermal zone that most likely contains a large number of secondary minerals, primarily montmorillonite and bentonite [31,34–36]. These sediments and rocks are high in porosity and are likely formed under conditions of a high water/rock ratio [37].



(**a**) (**b**)

Figure 1. (**a**) A map of the study area, located within the submarine hydrothermal system of Milos Island, which is situated in the central part of the Aegean Volcanic Arc in the Aegean Sea, Greece; (**b**) All fluid samples except cave fluid samples were collected in the Paleochori Bay. The figure was created using Ocean Data View software [38].

2.2. Sampling and Determinations

All vent fluids, except from the low-Cl cave fluid, were sampled from shallow (up to 10 m depth) underwater vents from the SE Milos Island (Paleochori Bay) during two expeditions, in 2002–2003 (Figure 1). Near Paleochori Bay, there are two springs with very low salinity and pH values. These springs discharge through rock cracks close to the sea level and are referred to as Cave samples. Detailed sampling information can be found in Wu et al. [23,27] and Lou et al. [21]. A total of thirty-four vent fluids, including four subaerial cave fluids from the 2002 expedition, a further two subaerial cave fluids, twenty-four submarine vent fluids, and four ambient seawaters from the 2003 expedition were selected for Mg isotopic determinations. All chemical experiments and procedures were conducted using a class-1000 clean room and a class-10 working bench, installed in the IGL lab at National Cheng-Kung University. Major and trace elements (e.g., Na, Cl, K, Ca, Mg, Li, B, S) were determined using inductively coupled plasma mass spectrometry (HR-ICP-MS, Thermo Scientific, Waltham, Ma USA, Element 2). After measuring the total sulfur (S) concentration using ICP-MS, the sulfate (SO_4^{2-}) concentration can be calculated based on the stoichiometric ratio of sulfur in sulfate. To minimize sample consumption (2–3 mL per sample was collected for all elemental and isotopic measurements), multiple elements were analyzed simultaneously using ICP-MS. The obtained analytical precision for major and trace elements was better than 3% (RSD).

Vent fluids were processed through ion-exchange chromatographic procedures to isolate Mg with high quantitative chemical yields [39]. The summary of Mg purification procedures is provided in Table S1, and the elution curve is shown in Figure S2. Briefly, about 1 mL cation exchange resin (BioRad AG 50W-X8, 200 to 400 meshes) (BioRad, Hercules, CA, USA) was loaded into an acid-cleaned PP column (5.5 mm in inner diameter and 7 cm in height). The resin was repeatedly cleaned using 30 mL 4 M HCl, then preconditioned with 3 mL 0.4 M HCl before loading the sample solution. Acids were prepared by sub-boiling distillation using quartz stills. Subsequently, approximately 1 µg Mg in 0.25 mL 0.4 M HCl was loaded into the column. Then, most of the major cations were separated through the subsequent additions of 28 mL 0.4 M HCl, 6 mL 0.15 M HF, 1 mL Milli-Q water (18.3 MΩ cm, MilliQ, Molsheim, France), 95% acetone-0.5 M HCl, 2 mL

Milli-Q, and 12 mL 1 M HCl, respectively. The Mg content was collected through the eluents in the final 12 mL 1 M HCl. These eluents were evaporated to dryness on a hot plate at 60~65°C then re-dissolved in 2% HNO_3 for Mg isotopic analysis.

Precise δ^{26}Mg was subsequently measured using multi-collector inductively coupled plasma mass spectrometer (MC-ICP-MS, Neptune, Thermo Scientific, Waltham, MA, USA), with detectors arranged to collect ^{24}Mg, ^{25}Mg, and ^{26}Mg at the same time, coupled with a de-solvation nebulizer system (APEX-IR, ESI), at the Department of Earth Sciences, National Cheng-Kung University and the Institute of Earth Sciences, Academia Sinica (Neptune PLUS, Thermo-Fisher Scientific, coupled with Aridus II, Cetac), Taiwan. The sample-standard bracketing procedure (SSB) was applied, and the sample solutions were bracketed using DSM-3 to correct for the instrumental mass bias of MC-ICP-MS.

Mg isotopes are expressed as:

$$\delta^{i}\text{Mg}\ (‰) = [(^{i}\text{Mg}/^{24}\text{Mg})_{\text{sample}}/(^{i}\text{Mg}/^{24}\text{Mg})_{\text{standard}} - 1] \times 1000, \quad (3)$$

where the i is 25 or 26, the standard represents DSM-3, an international reference material [40].

Long-term reproducibility was assessed based on duplicate Mg isotope analyses of the CAM-1 standard [40], yielding the mean δ^{25}Mg and δ^{26}Mg of -1.30 ± 0.06 and -2.54 ± 0.10‰ (2SD, n = 50), respectively. The value of δ^{25}Mg and δ^{26}Mg for IAPSO (reference seawater standard, S = 35; Ocean Scientific International Limited, Havant, UK) is -0.43 ± 0.05‰ and -0.85 ± 0.10‰ (2SD, n = 25), respectively. The three isotopes plot of δ^{26}Mg vs. δ^{25}Mg in samples and standards fitted well with linear regression, slopes 0.506 (Figure 2), indicating that they were all consistent with mass-dependence fractionation, and showed no detectable instrumental mass deviation [41].

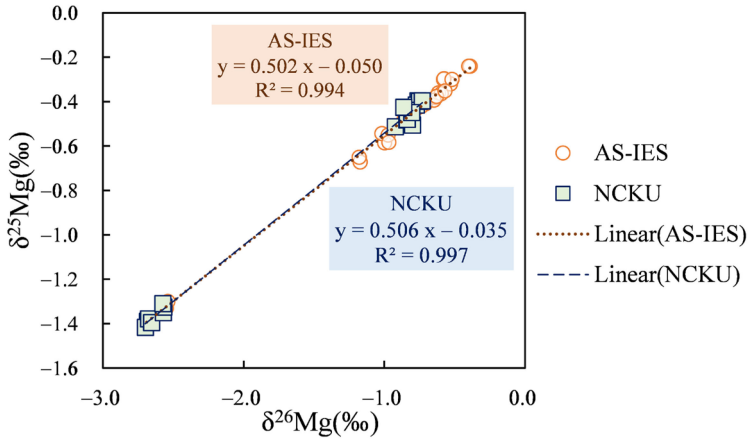


Figure 2. A plot of δ^{25}Mg vs. δ^{26}Mg obtained through measurements at the Institute of Earth Science, Academia Sinica (IESAS) and the Department of Earth Science, National Cheng Kung University (NCKU), with slopes of 0.502 and 0.506, respectively.

3. Results

All obtained vent fluid Mg isotopic compositions and available Li and B isotopic results, major and trace elements, temperature, and pH from the literature [21–23,27] are summarized in Tables 1 and 2. According to Huang et al. [13] and Kleint et al. [42], the main controlling factors of Mg content and δ^{26}Mg are temperature and pH, and these chemical characteristics were used to classify the vent fluids into three categories in Milos: (1) shallow circulation seawater-like fluids, which underwent intense water/rock interactions without phase separation, and had reacted at temperatures mostly between 90~110 °C and pH 5~7; (2) vapor-enriched fluids resulted from the deep circulation, such as the cave fluids

with pH < 2; (3) most submarine-brine fluids with pH < 5, generated by deep circulation, containing brines formed through phase separation and which exhibit a temperature–pH correlation, a phenomenon also reported in previous studies (Figure 3) [43]. These classifications are also based on information on the depth of circulation, volatile content, and phase separation provided by other studies [22,23,44]. Overall, the average Ca, Na, K, Cl, Sr, Li, B, and I in the Milos hydrothermal fluids is several orders of magnitudes higher than seawater. In contrast, their average Mg, SO_4^{2-} concentration is much lower. The average $\delta^{26}Mg$ in ambient seawater samples is –0.77‰, 2SD = 0.1‰ (n = 4), compared with the average seawater-like fluids, vapor-rich cave fluids, and submarine-brine fluids being –0.65~–1.00‰, –0.64~–1.18‰, and –0.52~−0.63‰, respectively (Table 2).

Table 1. Geochemical data from fluids collected at the Milos island during the 2003 expedition; some 2002 low-Mg Cave fluids are also included.

Sample No.	TYPE	SO_4 [1] (mM)	Ca [1] (mM)	Na [1] (mM)	Cl [1] (mM)	K [1] (mM)	pH [1]	Total Alkalinity [1] (mg/L)	T (°C) [1]	T (°C) [2]
03ML-1	Seawater	34	13	580	635	12	7.9	100	31.2	174.0
03ML-2	Seawater-like	36	13	590	660	13	5.5	65	106.7	176.0
03ML-4	Seawater	38	15	656	726	13	8.1	80	31.0	173.7
03ML-5	Cave	27	9	106	121	11	1.6	-	94.4	194.0
03ML-6	Cave	30	5	57	67	5	1.6	0.02	81.1	170.8
03ML-7	Submarine-brine	9	70	1058	1252	138	3.3	-	88.5	289.9
03ML-9	Submarine-brine	10	63	962	1128	122	3.7	-	78.3	286.4
03ML-10	Submarine-brine	10	61	1013	1185	122	4.1	-	82.7	323.3
03ML-12	Seawater-like	9	98	1324	1603	164	5.0	15	107.0	287.2
03ML-14	Seawater-like	11	79	1237	1454	161	4.9	-	114.2	292.6
03ML-15	Seawater-like	23	52	904	1060	82	6.6	60	62.5	261.2
03ML-16	Submarine-brine	8	100	1256	1460	155	5.3	30	68.7	285.4
03ML-18	Seawater-like	29	19	573	655	24	5.8	90	111.2	208.8
03ML-19	Seawater-like	22	23	543	626	34	5.7	40	104.2	231.6
03ML-20	Seawater-like	9	67	1098	1351	146	5.0	0	113.8	293.1
03ML-21	Seawater-like	27	33	702	821	47	6.1	90	112.2	237.7
03ML-22	Seawater-like	27	11	526	566	14	5.8	105	110.1	184.7
03ML-23	Submarine-brine	7	75	1170	1366	159	3.3	0	107.9	295.6
03ML-25	Seawater-like	22	12	495	546	20	4.6	-	110.3	209.3
03ML-26	Seawater-like	23	9	434	460	10	5.5	55	110.3	175.6
03ML-28	Seawater	35	13	577	626	12	8.1	95	29.0	174.6
03ML-29	Seawater-like	27	12	467	542	14	5.3	30	110.3	190.0
03ML-30	Seawater-like	11	33	716	837	80	5.5	10	111.9	276.9
03ML-31	Seawater-like	20	47	790	916	77	6.4	10	108.6	264.0
03ML-32	Submarine-brine	6	54	922	1068	122	3.9	-	81.3	290.9
03ML-33	Seawater	33	13	564	636	12	7.9	125	36.9	173.9
03ML-35	Submarine-brine	6	57	954	1095	132	3.4	-	96.8	295.2
03ML-37	Seawater-like	7	73	993	1192	123	5.2	-	108.0	283.6
03ML-39	Seawater-like	28	19	532	606	25	6.6	90	92.2	215.3
03ML-41	Seawater-like	26	11	466	507	12	5.6	60	111.9	183.4
02ML-4	Cave	29	9	88.78	128	13	1.8	-	91.4	303.5
02ML-5	Cave	37	6	45.46	65	7	1.6	-	78.2	288.1
02ML-29	Cave	28	9	91.28	125	13	1.7	-	91.0	190.0
02ML-30	Cave	34	5	49.37	68	7	1.8	-	90.0	276.9

Notes: [1]. Data from Wu et al. [22,23,27]. [2]. The in situ temperatures calculated using the Na-K-Ca geothermometer [45]. -: No data or below the detection limit.

Table 2. The isotopic compositions of Mg, Li, and B in the Milos fluids sampled during the 2003 expedition; some low-Mg Cave fluids from 2002 are also listed.

Sample No.	Type	Mg [1] (mM)	δ^{25}Mg (‰)	2SD	δ^{26}Mg (‰)	2SD	Li [2] (mM)	δ^{7}Li [2] (‰)	B [1] (mM)	δ^{11}B [1] (‰)
03ML-1	Seawater	65.8	−0.30	0.06	−0.58	0.10	0.0	31.5	0.5	38.19
03ML-2	Seawater-like	65.7	−0.38	0.06	−0.64	0.10	0.0	22.0	0.5	37.32
03ML-4	Seawater	73.1	−0.36	0.06	−0.61	0.10	0.0	29.8	0.5	38.16
03ML-5	Cave	2.7	−0.30	0.06	−0.58	0.10	0.6	4.7	0.4	3.64
03ML-6	Cave	2.2	−0.36	0.06	−0.60	0.10	0.2	4.3	0.2	4.21
03ML-7	Submarine-brine	12.1	−0.59	0.06	−1.00	0.10	6.9	5.7	4.5	4.43
03ML-9	Submarine-brine	16.7	−0.40	0.08	−0.76	0.10	6.4	4.7	4.1	4.48
03ML-10	Submarine-brine	21.9	−0.39	0.06	−0.65	0.10	6.3	5.7	4.1	4.93
03ML-12	Seawater-like	6.8	−0.42	0.11	−0.77	0.12	7.3	1.7	6.7	4.56
03ML-14	Seawater-like	15.9	−0.51	0.13	−0.92	0.16	7.9	4.6	5.1	4.43
03ML-15	Seawater-like	37.5	−0.47	0.06	−0.83	0.10	3.4	8.8	3.3	11.28
03ML-16	Submarine-brine	5.1	−0.40	0.10	−0.75	0.11	7.0	1.8	6.4	4.09
03ML-18	Seawater-like	54.5	−0.47	0.06	−0.82	0.10	0.6	5.6	1.0	24.99
03ML-19	Seawater-like	39.6	−0.48	0.07	−0.84	0.08	1.2	4.1	1.5	13.99
03ML-20	Seawater-like	13.4	−0.51	0.11	−0.80	0.16	7.2	2.1	4.4	5.06
03ML-21	Seawater-like	47.7	−0.48	0.06	−0.85	0.10	1.8	5.0	2.0	13.61
03ML-22	Seawater-like	50.7	−0.44	0.12	−0.84	0.15	0.2	9.1	0.4	30.22
03ML-23	Submarine-brine	10.3	−0.40	0.15	−0.73	0.20	7.4	8.7	4.9	4.39
03ML-25	Seawater-like	42.7	−0.67	0.06	−1.17	0.10	0.5	5.5	0.9	15.33
03ML-26	Seawater-like	43.2	−0.42	0.06	−0.74	0.10	0.0	21.3	0.3	36.51
03ML-28	Seawater	66.3	−0.54	0.06	−1.02	0.10	0.0	26.8	0.5	38.88
03ML-29	Seawater-like	51.3	−0.51	0.06	−0.90	0.10	0.2	6.8	0.7	24.28
03ML-30	Seawater-like	23.5	−0.51	0.06	−0.90	0.10	3.5	4.5	2.3	6.05
03ML-31	Seawater-like	31.2	−0.55	0.06	−0.97	0.10	3.1	4.2	3.0	10.92
03ML-32	Submarine-brine	11.3	−0.47	0.06	−0.84	0.10	5.5	3.9	3.5	4.63
03ML-33	Seawater	64.7	−0.48	0.06	−0.86	0.10	0.0	30.6	0.4	38.84
03ML-35	Submarine-brine	8.5	−0.48	0.13	−0.84	0.12	5.9	3.7	3.8	4.34
03ML-37	Seawater-like	8.5	−0.65	0.06	−1.18	0.10	5.5	4.1	5.0	9.13
03ML-39	Seawater-like	47.2	−0.45	0.16	−0.81	0.18	0.7	4.6	1.0	18.33
03ML-41	Seawater-like	50.4	−0.43	0.12	−0.86	0.16	0.1	7.0	0.5	34.93
02ML-4	Cave	1.8	−0.30	0.06	−0.52	0.10	0.8	4.7	0.6	6.68
02ML-5	Cave	1.3	−0.58 *	0.06	−0.97 *	0.10	0.3	4.7	0.3	7.24
02ML-29	Cave	1.8	−0.38	0.06	−0.63	0.10	0.7	4.3	0.6	4.90
02ML-30	Cave	1.7	−0.35	0.06	−0.57	0.10	0.3	4.6	0.3	6.57

Notes: [1]. Data from Wu et al. [22,23,27]. [2]. Data from Lou et al. [21]. * Ca/Mg > 0.2, no δ^{26}Mg correction.

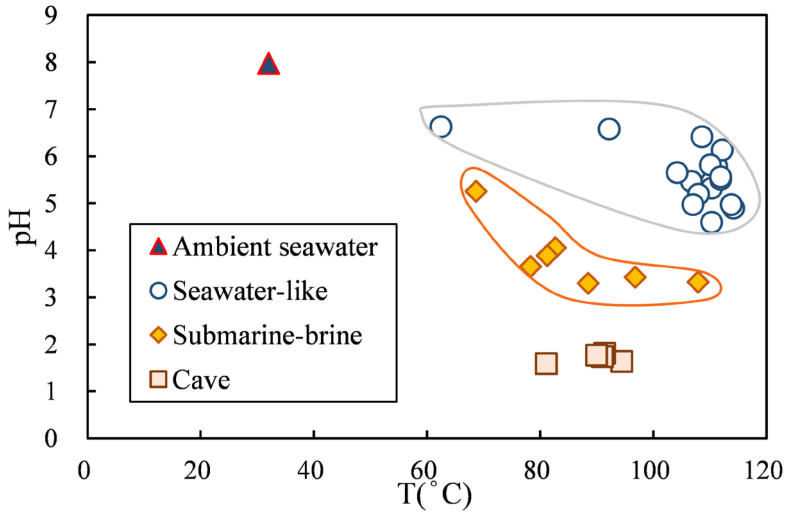


Figure 3. A plot of temperature vs. pH in vent fluids collected from the Milos hydrothermal system.

4. Discussion

4.1. Chemistry of Milos Hydrothermal Fluids

The Mediterranean Sea is a semi-closed basin, easily influenced by evaporation or dilution conditions [46,47]. The Mg concentration in ambient seawater varied largely, up to 15 mM in 2002 and 2003; these results agree with previous surveys [48] (Figure 4). Additionally, these values may also be affected by a tidal mixing process [49]. For this reason, we discuss the geochemical data separately for different years. In the following discussion, the average seawater sampled during 2003 is used as a seawater endmember, since most of the samples analyzed are from 2003, with only a few cave samples from 2002 included.

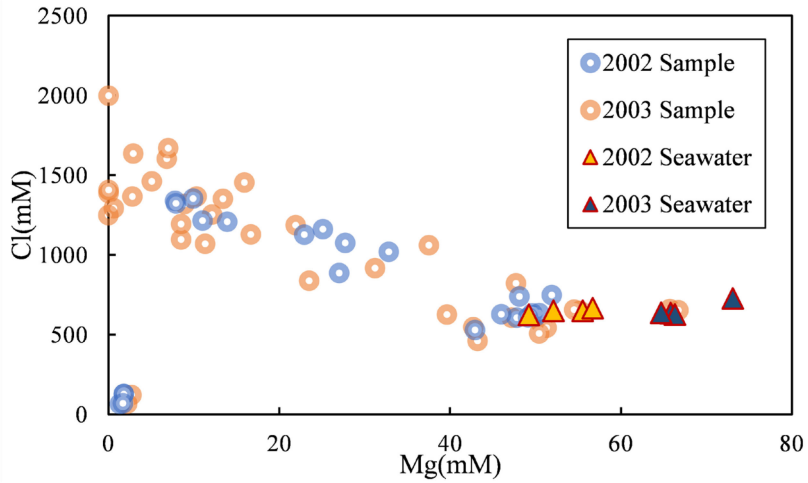


Figure 4. A plot showing Mg vs. Cl in seawater and vent fluids sampled during 2002/2003 expeditions.

Potential water sources in hydrothermal fluids include meteoric, seawater, groundwater, magmatic water, or other continental margin-derived fluids [48,50,51]. The shallow circulation is predominantly affected by seawater or groundwater, while the deep reservoirs are primarily affected by magmatic water in Milos Island [21,22].

The distributions of major elements of Na, Ca, and Cl are inversely proportional to Mg in the Milos fluids (Figure 5A–C). Other major elements, besides Mg and SO_4^{2-}, are correlated positively with each other, consistent with a linear mixing process between seawater and hydrothermal endmembers (Figure 5D). The results indicate that an additional endmember with low Mg is needed to explain the tendency in most hydrothermal specimens, where cave fluids trend toward the origin point (asterisk). Previous studies have proposed a mixing model among zero-Mg magmatic fluids, seawater, and groundwater at shallow reservoirs [22,48,50].

These figures show at least three sources affecting the shallow-water hydrothermal system in Milos: (1) ambient seawater; [Mg] = 67.5 mM, [Cl] = 655.9 mM, (2) hydrothermal endmember (zero-Mg and the highest Cl); [Mg] = 0 mM, [Cl] = 1709.6 mM (referring to the calculation method of Bischoff and Dickson [52] and Pichler et al. [53], and (3) magmatic H_2O fluids [50] and groundwater [22,48]; [Mg] = 0 mM, [Cl] = 0 mM. The green dashed line suggests the mixing trend of seawater and the potential hydrothermal endmembers.

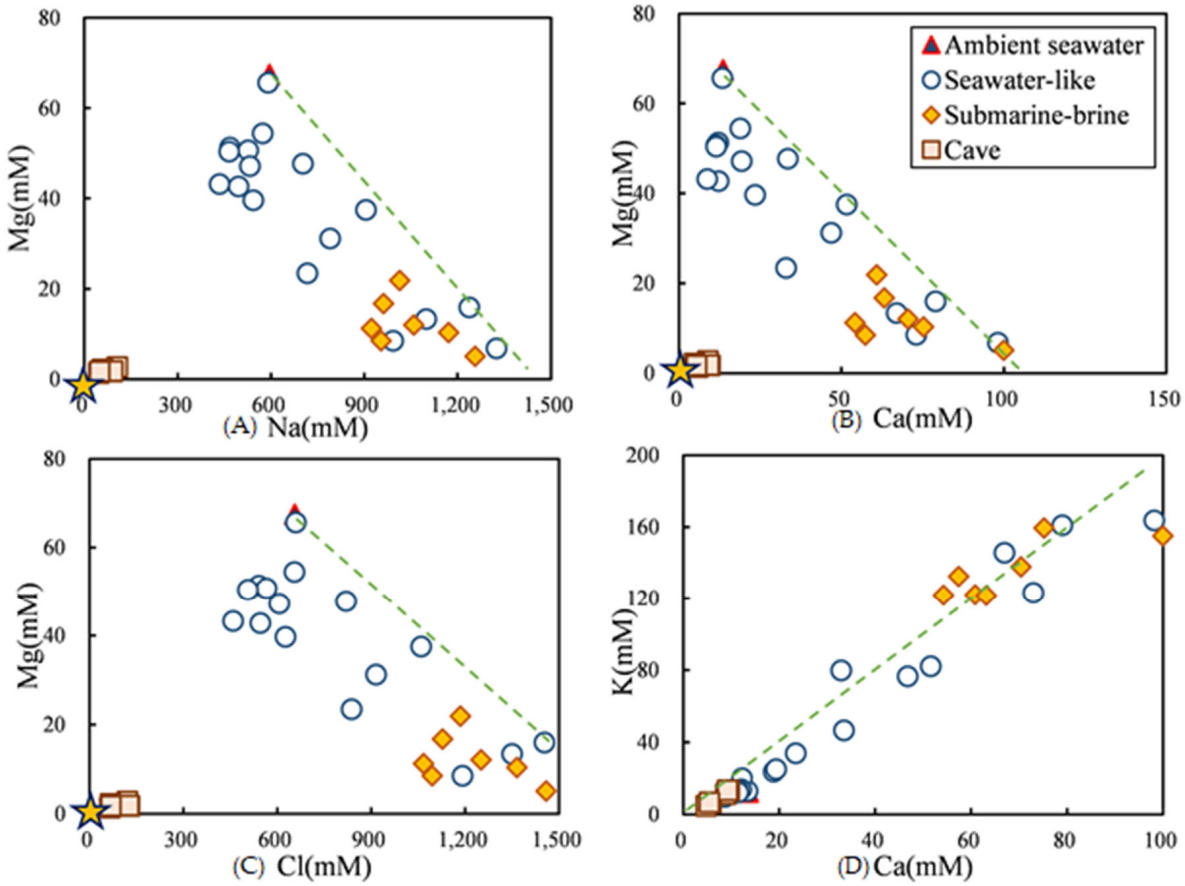


Figure 5. Plots showing Mg vs. major element concentrations for (**A**) Na, (**B**) Ca, and (**C**) Cl, as well as (**D**) K vs. Ca, indicative of a three-endmember mixing. The asterisk represents the endmember with low Mg.

4.2. Influence of Carbonate Mineral Formation on Mg Isotopic Fractionation

Carbonate minerals, such as calcite and dolomite, display much lighter δ^{26}Mg values (−1.05 to −4.85‰) compared to silicates (0.02 to −1.09‰) due to significant Mg isotopic fractionation during crustal alteration. Heavy Mg isotopes preferentially incorporate into minerals at intermediate temperatures [13–19]. This makes δ^{26}Mg a highly effective tracer for water–rock interactions in low-temperature hydrothermal environments [13].

Shallow-circulation, seawater-like fluids in Milos are characterized by intense water–rock interactions without phase separation, with reaction temperatures of 90–110 °C, pH values of 5–7, and δ^{26}Mg values ranging from −0.64 to −1.18‰ (Table 2). To assess the impact of carbonate mineral formation on Mg isotopic fractionation in these fluids, this study used the PHREEQC database to model various mineral saturation indices (SI), where SI = log (IAP/Ksp), with IAP being the Ion Activity Product of the mineral, and *Ksp* being the equilibrium constant of the mineral under specific temperature and pressure conditions. SI > 0 indicates conditions favorable for precipitation, while SI < 0 favors dissolution [54]. PHREEQC (Version 3) is a widely used geochemical modeling software developed by the U.S. Geological Survey (USGS). While it is primarily designed for low-temperature aqueous geochemistry, several previous studies have successfully applied PHREEQC to simulate mineral saturation in high-temperature hydrothermal systems, such as those by Sætre et al. [55] and Hall et al. [56].

Three carbonate minerals were focused on, namely, calcite, aragonite, and dolomite, because carbonate minerals contain lighter magnesium isotopes compared to silicate minerals [12]. Their precipitation significantly impacts the magnesium isotopic composition of hydrothermal fluids [13]. These hydrothermal fluids mostly underwent water/rock reactions at various depths, where the Na-K-Ca geo-thermometer was applied to estimate their in situ reaction temperatures [45].

$$t\ ^{\circ}C = \frac{1647}{\log(Na/K) + \beta\left(\sqrt{Ca}/Na\right) + 2.24} - 273.15, \quad (4)$$

$$\beta = \frac{4/3 \text{ for } Ca^{1/2}}{Na} > 1, \text{ and } t < 100\ ^{\circ}C; \beta = \frac{1/3 \text{ for } Ca^{1/2}}{Na} > 1, \text{ and } t_{4/3} > 100\ ^{\circ}C \quad (5)$$

The fluid compositions from the three categories were used to calculate saturation indices (SI). Most carbonate minerals had SI < 0, indicating dissolution, except for anhydrite in the submarine-brine and seawater-like fluids, which showed positive SI values (Table 3). The surface sediments in Paleochori Bay comprise only 0.02% carbonate [32]. This, combined with the SI < 0, suggests that the impact of carbonate formation on $\delta^{26}Mg$ can be ignored. Additionally, SI > 0 for anhydrite is consistent with the previous conclusion that anhydrite should be precipitated at T > 150 °C [43,44,57]. Detailed examination of cores and cuttings from the two drill sites, obtained from a depth of about 1100 m in Milos geothermal field shows that the hydrothermal minerals occurring in the rock include anhydrite [58].

Table 3. The mineral saturation indices were calculated using PHREEQC.

Mineral SI	Submarine-Brine	Cave	Seawater-Like		
Sample no.	03ML-16	03ML-6	03ML-2	03ML-12	03ML-18
T(°C)-(Na-K-Ca)	285.4	170.8	176.0	287.2	208.8
Anhydrite ($CaSO_4$)	1.53 [1]	−0.55	0.74 [1]	1.55 [1]	1.01 [1]
Gypsum ($CaSO_4 \cdot 2H_2O$)	−0.24	−15.61	−0.27	−0.23	−0.23
Aragonite ($CaCO_3$)	−2.75	−17.23	−0.63	−3.20	−0.21
Calcite ($CaCO_3$)	−2.71	−17.16	−0.56	−3.16	−0.15
Dolomite ($CaMg(CO_3)_2$)	−13.66	−36.48	−2.54	−14.52	−3.15

Note: [1] Mineral SI values greater than 0, indicating super-saturation.

4.3. Mg Isotopic Variation in Vent Fluids

4.3.1. The Seawater-like Fluids

Variations in magnesium concentration within hydrothermal fluids indicate that the formation of secondary minerals, whether within the lattice structure or the mineral interlayer, could lead to substantial magnesium depletion from the discharge fluid. To explore the fractionation mechanism of seawater-like hydrothermal fluids, a Rayleigh fractionation model was chosen for more in-depth discussion. Rayleigh fractionation is presented in the equation below [59]:

$$\delta^{26}Mg = (\delta^{26}Mg_0 + 1000) \times f^{(\alpha-1)} - 1000, \quad (6)$$

where $\delta^{26}Mg_0$: initial $\delta^{26}Mg$ (average 2003 ambient seawater)

f: the ratio of Mg remaining in the liquid, calculated from $Mg_{\text{liquid sample}}/Mg_{\text{seawater}}$

α: fractionation factor, $\alpha^{26/24}_{solid-liquid}$ $(^{26}Mg_{solid}/^{24}Mg_{solid})/(^{26}Mg_{liquid}/^{24}Mg_{liquid})$; all α mentioned in this study are $\alpha^{26/24}_{solid-liquid}$.

Plugging the seawater-like group data into the formula reveals a wide range of α values at low Mg fractions, while most samples with relatively high Mg fractions align closely with the α = 1.00020 curve (Figure 6). Sample 03ML-2 was excluded because its Mg value was close to that of ambient seawater. Even within the error margin, the variation in α remains significant, highlighting the combined influence of Mg-rich mineral dissolution and secondary mineral formation on Mg isotopic compositions. Quantifying fractionation factors during clay formation is challenging. For instance, fractionation factors for saprolites from South Carolina, calculated using the Rayleigh distillation method, range from 1.00005 to 1.00040 [59]. Generally, α is greater than or equal to 1, which means heavy isotopes preferentially enter a solid phase of silicates. The α of Milos seawater-like fluids differs from the original estimated α of bentonite, 1.00040 [17]. Three possibilities can be used to explain this observation: (1) Unknown chlorite may have formed under the seabed of Milos island, significantly affecting δ^{26}Mg in vent fluid. A potential source for this may be limited basement outcrops composed of weakly metamorphosed rocks of quartz, muscovite, and chlorite, as reported in the literature [58,60]; (2) There may be an infiltration of seawater, resulting in seawater-like δ^{26}Mg in the vent fluids; (3) The parameters of the reaction, such as w/r, pH, and pressure, may have indirectly affected the fractionation coefficient [15,17]. It is difficult to fix ambient conditions in nature, and the calculated fractionation coefficient may not fully represent a mineral species. Any future drilling plan in this area will provide an opportunity to establish more comprehensive water/rock reaction models.

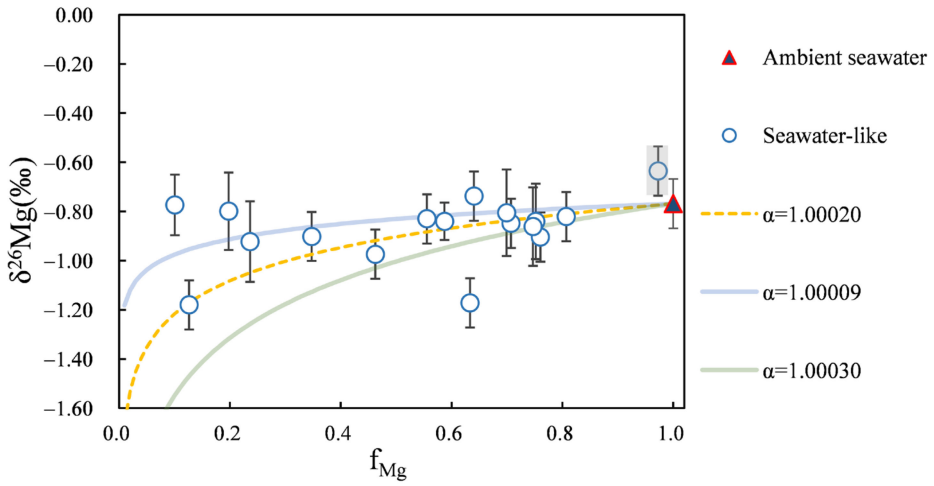


Figure 6. A plot of f_{Mg} vs. δ^{26}Mg in the seawater-like vent fluids sampled from Milos. Two trend lines, the blue and green lines, are values obtained after accounting for analytical error (SD).

Laboratory experiments indicated that Mg incorporated into the octahedral sheet of clay minerals (such as chlorite) is isotopically heavier than surface-bound or exchangeable components observed during acetic-acid leach tests. In contrast, exchangeable Mg, measured in neutral-pH NH_4Cl solutions, is consistently isotopically lighter than the bulk clay mineral's δ^{26}Mg value [18]. For instance, at pH = 1, the dissolution of "structural Mg" causes δ^{26}Mg in the fluid to become heavier. In contrast, at pH = 5, dissolution is primarily influenced by "exchangeable Mg", resulting in lighter δ^{26}Mg values in the fluid [15,18,61]. However, this phenomenon is not documented in natural hydrothermal systems. Our samples show no significant correlation between pH and α, suggesting that the Mg isotopic fractionation mechanism in seawater-like fluids results from a combination of secondary mineral formation/dissolution and pH effects.

4.3.2. Deep Circulation-Vapor and Brine Phase

In the Milos system, phase separation produces vapors and brines associated with deep circulation. Liquid and vapor phases were sampled from a deep well (M-2, 1381 m depth) in the Zephyria plain on Milos Island. The chemical composition of condensed vapor samples showed low concentrations of major elements, with values of Na = 16 mmol/L, Cl = 21 mmol/L, and Mg = 0.0004 mmol/L [58]. The influence of phase separation on Mg isotopic fractionation in the Milos system remains unclear. However, the Milos results suggest that the low-Cl vapor phase has preferentially taken up heavy δ^{26}Mg, deviating by up to 0.25‰ from the seawater value, while no significant changes are observed in the brines (Figure 7). Two possible explanations for this observation are (1) multiple mixing events, such as the dissolution of previously formed anhydrite deposits with low Mg content but relatively positive δ^{26}Mg compared to carbonate minerals (e.g., dolomite), which may occur during the upflow process when fluid temperatures fall below anhydrite stability thresholds [57,62], or (2) minor fractionation caused by high reservoir temperatures during phase separation; however, recent findings suggest it is negligible under high-temperature conditions [63]. The former hypothesis may be supported by the observation of high Ca and SO_4^{2-} but low Mg concentrations, coupled with under-saturation in low-Cl Cave fluids (Table 3) [23]. At high temperatures, changes in δ^{26}Mg in deep circulation brines are primarily driven by removal mechanisms, such as mineral formation. Consequently, the effects of host rock composition, secondary mineral formation, and phase separation on δ^{26}Mg values in brines are minimal [63].

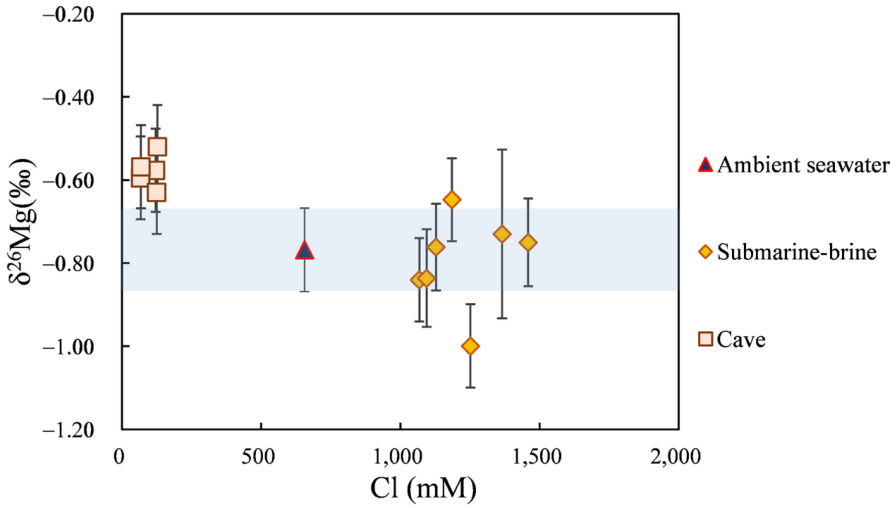


Figure 7. Plot of Cl concentration vs. δ^{26}Mg in the deep circulation fluids in Milos.

4.3.3. Combined Mg, B, and Li Isotopes in Vent Fluids

Below, we combine our new Mg isotopic results with the published δ^{7}Li and δ^{11}B in Milos fluids, previously measured in our laboratory [21–23] to facilitate further discussion. δ^{26}Mg and δ^{7}Li are two isotopic systems that are often discussed together in chemical weathering. Furthermore, well-documented negative correlation associated with secondary minerals tend to preferentially absorb light δ^{7}Li and heavy δ^{26}Mg during water/rock interaction at low temperatures [64]. However, the δ^{7}Li changes are less clear due to the high reservoir temperature in Milos (Figure 8). The δ^{7}Li values in hydrothermal fluid fall in a range of +1.7~+31.5‰, indicating the mixing of two endmember components, namely, hydrothermal brine fluids and seawater [21]. The hydrothermal brine values appear to be predominately affected by the dissolution of primary rocks without isotopic fractionation, rather than secondary minerals formation at high temperatures. Therefore,

the δ^7Li in hydrothermal fluids represent the geochemical signature of protoliths rather than a secondary processes [64].

The δ^{11}B varies from +3.64 to +37.32‰ in the Milos hydrothermal fluids (Figure 8; Table 2). The ranges of the δ^{11}B values in the deep circulation-vapor and brine phase are +3.64 and +7.24‰, respectively (Table 2). This δ^{11}B value in the vapor is close to the volcanic rocks or magmatic water, δ^{11}B = −2.0‰ and −2.5‰, respectively [65]. According to Daskalopoulos et al. [66], the predominant component of local emissions is CO_2 in the area, reaching as high as 91–94% vol. However, experimental evidence suggests that increasing the amount of carbon dioxide in solution will shift the seawater boiling curve, making the fluid prone to boiling [24,25]. Therefore, the deep hydrothermal fluids from Milos Island are more susceptible to reaching subcritical points and undergoing phase separation due to the influence of gases. In contrast, the seawater-like samples show a wide range of δ^{11}B = +4.43~+37.32‰, with in situ temperatures being lower than the subcritical point and thus not linked to phase separation. The variation of δ^{11}B values in seawater-like fluids could have resulted from its rather high pH, 5~7, where predominant isotopic fractionation occurs via equilibrium exchange between two aqueous species of $B(OH)_3$ and $B(OH)_4^-$ [67–69]. This supports the conclusion that Mg isotopic fractionation in seawater-like fluids results from a combination of secondary mineral formation/dissolution and pH effects. At pH = 5~7, dissolution is primarily influenced by "exchangeable Mg", leading to lighter δ^{26}Mg values in the fluid [15,18,61].

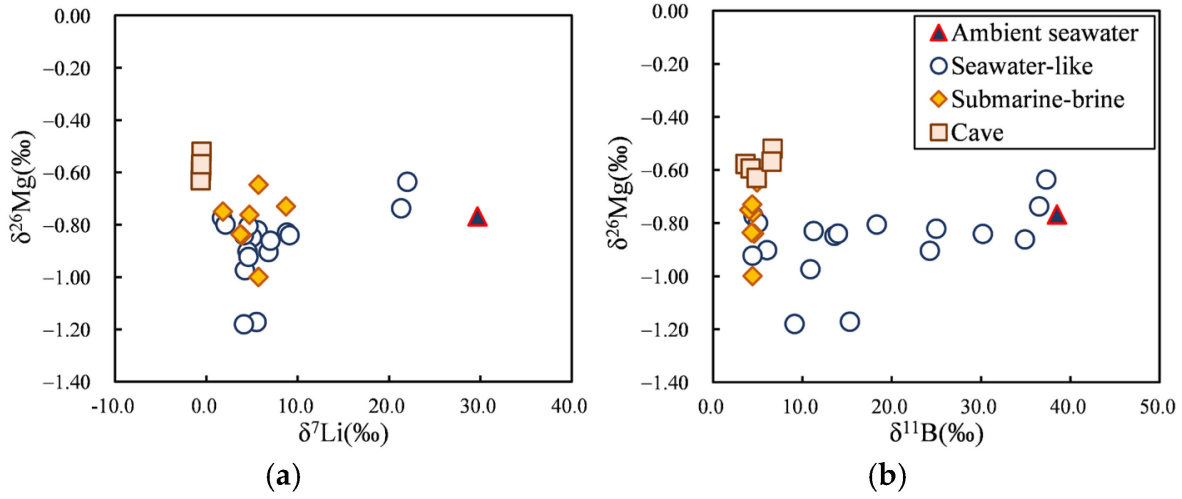


Figure 8. The plots of δ^{26}Mg vs. (**a**) δ^7Li and (**b**) δ^{11}B in the vent fluids sampled from Milos.

Integrating with the available literature B isotope results, a summary diagram for depicting the submarine hydrothermal processes is presented (Figure 9). The controlled factors of δ^{26}Mg fractionation mechanisms are phase separation, water/rock interactions, and various sources mixing in shallow-water hydrothermal systems. Three dominant fluid types are identified in this region: (a) Cave fluids: Characterized by extremely low pH (<1.9), very low Mg (1.9 mM), and relatively heavy δ^{26}Mg (−0.58‰) compared to ambient seawater. (b) High-Cl brines: Contain high major element concentrations, Mg (12.3 mM), and light δ^{26}Mg (−0.79‰). At high temperatures, δ^{26}Mg variations are primarily influenced by mineral formation mechanisms. (c) Seawater-like fluids: High Mg (37.1 mM) with seawater-like Cl and δ^{26}Mg (−0.87‰), likely influenced by secondary mineral formation/dissolution and pH effects. At pH 5–7, dissolution is dominated by "exchangeable Mg", leading to lighter δ^{26}Mg values [15,18,61].

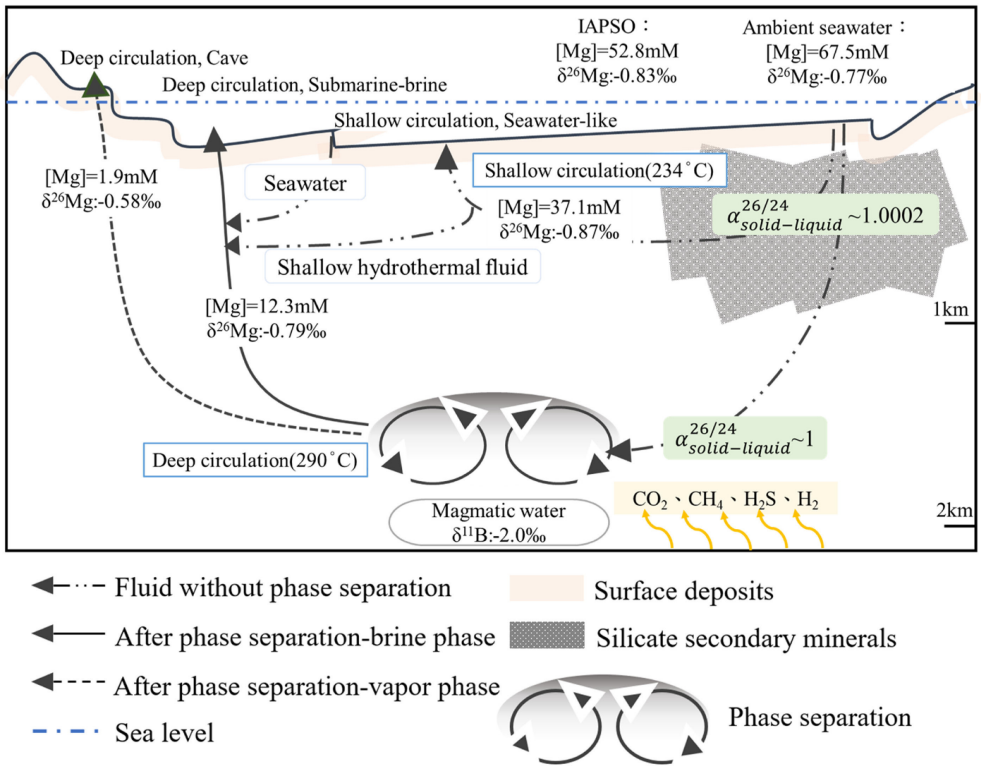


Figure 9. A schematic drawing showing the Mg isotopic composition variations and possible geochemical processes occurring in the shallow-water hydrothermal system in Milos Island. Data shown in the diagram are the average values of Mg and δ^{26}Mg.

4.4. Global Data Comparisons

Until recently, there have been no δ^{26}Mg data in the hydrothermal MARHYS database [3]. Only two studies have addressed the δ^{26}Mg in hydrothermal fluids (Table 4; Figure 10). Wilckens et al. [50] found no fractionation in vent fluids and no samples with Mg < 20 mM in their study. Eom et al. [63] reported some degree of Mg isotopic fractionation in their study, namely, a fractionation factor of 1.00008 (Table 4). The fluid temperatures in this study range from 60 to 110 °C, compared to 200 to 320 °C in Eom et al. [63], which agrees with previous observations of a small fractionation factor at high temperatures [17]. This confirms that the Mg isotope of low-temperature hydrothermal systems is a more suitable tool for deciphering water/rock interactions. Our study shows a different trend in Mg isotope values, especially in Cave fluids, under phase separation, mineral removal/formation, and secondary mineral formation/dissolution conditions compared to the deepwater hydrothermal systems (e.g., Mariana Trough and Okinawa Trough), suggesting that the former fluids are influenced by additional processes besides phase separation. Deep geothermal samples of the phase-separated type exhibit distinct chemical characteristics, with Cl concentrations ranging from 302 to 452 mM, pH at 4.7, and minimal Mg isotopic fractionation. In contrast, Milos cave fluids, referred to as vapor-enriched fluids, have Cl concentrations of 65 to 128 mM and a pH < 2 (Figure 10). Deepwater hydrothermal systems may have been affected by mixing with other sources, resulting in high pH and high Cl.

Table 4. Comparison of fractionation factor, measured temperature, and pH in different hydrothermal system [50,63]. (Fractionation factor: $\alpha^{26/24}_{solid-liquid}$).

Location, Hydrothermal System	Fractionation Factor (α)	Temperature (°C)	pH
The Manus Basin, acid sulfate (white smoker) systems [50]	No fractionation	47~241	0.9~2.4
The western Pacific, arc, and back-arc hydrothermal systems [63]	1.00008	200~320	2.5~5.3
The Milos Island, shallow-water hydrothermal systems (seawater-like fluids, this study)	1.00020	63~114	4.6~6.6

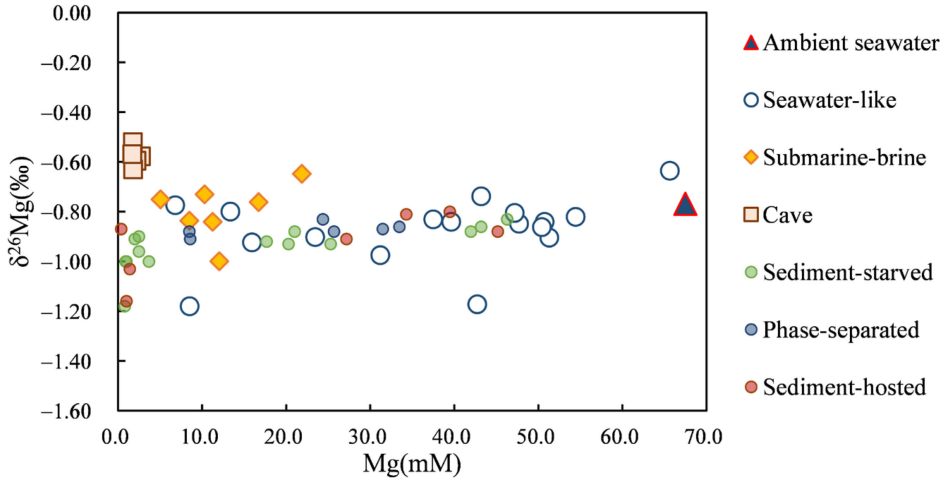


Figure 10. A plot showing Mg vs. δ^{26}Mg in vent fluids in Milos. The samples from Eom et al. [63] are denoted by a solid circle.

5. Conclusions

Initially relying on pH and temperature in hydrothermal fluids collected from the Milos system, three subgroups have been identified: vapor-dominated deep circulation (cave), brine-dominated deep circulation, and shallow seawater-like fluids. This grouping was tested using the degree of water/rock interactions as recorded in the values for Mg concentration and δ^{26}Mg. The variation in elemental concentrations shows a complex fluid mixing among groundwater, seawater, hydrothermal fluid, and magmatic H_2O fluids. The δ^{26}Mg in seawater-like fluids, ranging from −0.64~−1.18‰, mostly follows a Rayleigh fractionation trend, with a fractionation factor α = 1.00020 ± 0.00011. The δ^{26}Mg in cave fluids and submarine brines have values of −0.52~−0.63‰ and −0.65~−1.00‰, respectively. Our results indicate that the vapor phase is preferentially taking up heavy Mg isotopes; however, no significant changes in the brine phase are observed, potentially due to multiple seawater mixing incidents. Compared with other available isotopic systems, the data from Milos suggest that Mg isotopes are more suitable for exploring water/rock interactions in low-temperature hydrothermal systems.

Supplementary Materials: The following supporting information can be downloaded at: https://www.mdpi.com/article/10.3390/w17030370/s1, Figure S1: Mg isotope fractionation in silicate/water systems; Figure S2: Elition curve; Table S1: Mg purification method.

Author Contributions: Conceptualization: C.-F.Y. and Y.-C.C.; methodology: Y.-C.C. and C.-H.C.; validation: Y.-C.C. and C.-F.Y.; investigation: Y.-C.C., C.-H.C. and E.V.-J.; writing—original draft preparation: Y.-C.C.; writing—review and editing: Y.-C.C., K.-F.H., S.-F.W., C.-F.Y., E.V.-J., E.B. and C.-H.C.; supervision: C.-F.Y.; project administration: C.-F.Y. All authors have read and agreed to the published version of the manuscript.

Funding: This research was funded by NSC, grant number 104-2611-M-006-003 and 104-2116-M-006-005 to C.-F.Y. This research was funded by MOST and MOE, grant number D104-32A02 to C.-F.Y. This

research was funded by NGC, grant number 7049-01 to S.A.R.G of the National and Kapodistrian University of Athens (E.B.). Fieldwork was funded by the National Geographic Society (NGC grant 7049-01) and the Natural History Museum (E.V.-J).

Data Availability Statement: Data are contained within the article.

Acknowledgments: We thank the three reviewers and the editor for providing us with constructive comments/suggestions in the earlier draft, which have improved this paper significantly.

Conflicts of Interest: The authors declare no conflicts of interest.

References

1. Baker, E.T.; German, C.R. On the global distribution of hydrothermal vent fields. *Geophys. Monogr. Ser.* **2004**, *148*, 245–266.
2. Beaulieu, S.E.; Baker, E.T.; German, C.R.; Maffei, A. An authoritative global database for active submarine hydrothermal vent fields. *Geochem. Geophys. Geosyst.* **2013**, *14*, 4892–4905. [CrossRef]
3. Diehl, A.; Bach, W. MARHYS (MARine Hydrothermal Solutions) Database: A Global Compilation of Marine Hydrothermal Vent Fluid, End Member, and Seawater Compositions. *Geochem. Geophys. Geosyst.* **2020**, *21*, e2020GC009385. [CrossRef]
4. Tarasov, V.G.; Gebruk, A.V.; Mironov, A.N.; Moskalev, L.I. Deep-sea and shallow-water hydrothermal vent communities: Two different phenomena? *Chem. Geol.* **2005**, *224*, 5–39. [CrossRef]
5. Voudouris, P.; Kati, M.; Magganas, A.; Keith, M.; Valsami-Jones, E.; Haase, K.; Klemd, R.; Nestmeyer, M. Arsenian pyrite and cinnabar from active submarine nearshore vents, Paleochori Bay, Milos Island, Greece. *Minerals* **2021**, *11*, 14. [CrossRef]
6. Martelat, J.E.; Escartín, J.; Barreyre, T. Terrestrial shallow water hydrothermal outflow characterized from out of space. *Mar. Geol.* **2020**, *422*, 106119. [CrossRef]
7. Zhang, Z.; Fan, W.; Bao, W.; Chen, C.T.A.; Liu, S.; Cai, Y. Recent developments of exploration and detection of shallow-water hydrothermal systems. *Sustainability* **2020**, *12*, 9109. [CrossRef]
8. Rosman, K.J.R.; Taylor, P.D.P. Isotopic compositions of the elements 1997 (Technical Report). *Pure Appl. Chem.* **1998**, *70*, 217. [CrossRef]
9. Guo, B.; Zhu, X.; Dong, A.; Yan, B.; Shi, G.; Zhao, Z. Mg isotopic systematics and geochemical applications: A critical review. *J. Asian Earth Sci.* **2019**, *176*, 368–385. [CrossRef]
10. Carpenter, J.H.; Manella, M.E. Magnesium to chlorinity ratios in seawater. *J. Geophys. Res.* **1973**, *78*, 3621–3626. [CrossRef]
11. Ling, M.-X.; Sedaghatpour, F.; Teng, F.-Z.; Hays, P.D.; Strauss, J.; Sun, W. Homogeneous magnesium isotopic composition of seawater: An excellent geostandard for Mg isotope analysis. *Rapid Commun. Mass Spectrom.* **2011**, *25*, 2828–2836. [CrossRef] [PubMed]
12. Young, E.; Galy, A. The isotope geochemistry and cosmochemistry of magnesium. *Rev. Mineral. Geochem.* **2004**, *55*, 197–230. [CrossRef]
13. Huang, K.-J.; Teng, F.-Z.; Plank, T.; Staudigel, H.; Hu, Y.; Bao, Z.-Y. Magnesium isotopic composition of altered oceanic crust and the global Mg cycle. *Geochim. Cosmochim. Acta* **2018**, *238*, 357–373. [CrossRef]
14. Li, W.; Beard, B.L.; Li, C.; Johnson, C.M. Magnesium isotope fractionation between brucite [$Mg(OH)_2$] and Mg aqueous species: Implications for silicate weathering and biogeochemical processes. *Earth Planet. Sci. Lett.* **2014**, *394*, 82–93. [CrossRef]
15. Ryu, J.-S.; Vigier, N.; Decarreau, A.; Lee, S.-W.; Lee, K.-S.; Song, H.; Petit, S. Experimental investigation of Mg isotope fractionation during mineral dissolution and clay formation. *Chem. Geol.* **2016**, *445*, 135–145. [CrossRef]
16. Teng, F.-Z.; Li, W.-Y.; Rudnick, R.L.; Gardner, L.R. Contrasting lithium and magnesium isotope fractionation during continental weathering. *Earth Planet. Sci. Lett.* **2010**, *300*, 63–71. [CrossRef]
17. Voigt, M.; Pearce, C.R.; Fries, D.M.; Baldermann, A.; Oelkers, E.H. Magnesium isotope fractionation during hydrothermal seawater-basalt interaction. *Geochim. Cosmochim. Acta* **2020**, *272*, 21–35. [CrossRef]
18. Wimpenny, J.; Colla, C.A.; Yin, Q.-Z.; Rustad, J.R.; Casey, W.H. Investigating the behaviour of Mg isotopes during the formation of clay minerals. *Geochim. Cosmochim. Acta* **2014**, *128*, 178–194. [CrossRef]
19. Shao, H.; Yang, S.; Dong, A.; Hu, Z. Magnesium isotopes of chlorite-rich hydrothermal sediments in the Okinawa Trough and indications for Mg cycle. *Sci. China Earth Sci.* **2023**, *66*, 648–662. [CrossRef]
20. Vigier, N.; Decarreau, A.; Millot, R.; Carignan, J.; Petit, S.; France-Lanord, C. Quantifying Li isotope fractionation during smectite formation and implications for the Li cycle. *Geochim. Cosmochim. Acta* **2008**, *72*, 780–792. [CrossRef]
21. Lou, U.T.; Wu, S.F.; You, C.F.; Chung, C.H.; Valsami-Jones, E.; Baltatzis, E. Lithium isotope systematics and water/rock interactions in a shallow-water hydrothermal system at Milos Island, Greece. *Mar. Chem.* **2023**, *257*, 104327. [CrossRef]
22. Wu, S.F.; You, C.F.; Wang, B.S.; Valsami-Jones, E.; Baltatzis, E. Two-cells phase separation in shallow submarine hydrothermal system at Milos Island, Greece: Boron isotopic evidence. *Geophys. Res. Lett.* **2011**, *38*, 5. [CrossRef]

23. Wu, S.-F.; You, C.-F.; Lin, Y.-P.; Valsami-Jones, E.; Baltatzis, E. New boron isotopic evidence for sedimentary and magmatic fluid influence in the shallow hydrothermal vent system of Milos Island (Aegean Sea, Greece). *J. Volcanol. Geotherm. Res.* **2016**, *310*, 58–71. [CrossRef]
24. Monecke, T.; Petersen, S.; Hannington, M.D. Constraints on water depth of massive sulfide formation: Evidence from modern seafloor hydrothermal systems in arc-related settings. *Econ. Geol.* **2014**, *109*, 2079–2101. [CrossRef]
25. Shi, X.; Shi, L.; Yan, Q.; Ye, J. Hydrothermal activities and mineralization in the arc and back-arc basin systems, Western Pacific. *J. Jilin Univ. (Earth Sci. Ed.)* **2016**, *46*, 1124–1138.
26. Butterfield, D.A.; Massoth, G.J.; McDuff, R.E.; Lupton, J.E.; Lilley, M.D. Geochemistry of hydrothermal fluids from Axial Seamount hydrothermal emissions study vent field, Juan de Fuca Ridge: Subseafloor boiling and subsequent fluid-rock interaction. *J. Geophys. Res. Solid Earth* **1990**, *95*, 12895–12921. [CrossRef]
27. Wu, S.-F.; You, C.-F.; Valsami-Jones, E.; Baltatzis, E.; Shen, M.-L. Br/Cl and I/Cl systematics in the shallow-water hydrothermal system at Milos Island, Hellenic Arc. *Mar. Chem.* **2012**, *140–141*, 33–43. [CrossRef]
28. Khimasia, A.; Renshaw, C.E.; Price, R.E.; Pichler, T. Hydrothermal Flux and Porewater Geochemistry in Paleochori Bay, Milos, Greece. *Chem. Geol.* **2021**, *571*, 120188. [CrossRef]
29. Gilhooly, W.P.; Fike, D.A.; Druschel, G.K.; Kafantaris, F.C.A.; Price, R.E.; Amend, J.P. Sulfur and oxygen isotope insights into sulfur cycling in shallow-sea hydrothermal vents, Milos, Greece. *Geochem. Trans.* **2014**, *15*, 19. [CrossRef]
30. Fytikas, M.; Innocenti, F.; Kolios, N.; Manetti, P.; Mazzuoli, R.; Poli, G.; Rita, F.; Villari, L. Volcanology and petrology of volcanic products from the island of Milos and neighbouring islets. *J. Volcanol. Geotherm. Res.* **1986**, *28*, 297–317. [CrossRef]
31. Köster, M.H.; Williams, L.B.; Kudejova, P.; Gilg, H.A. The boron isotope geochemistry of smectites from sodium, magnesium and calcium bentonite deposits. *Chem. Geol.* **2019**, *510*, 166–187. [CrossRef]
32. Megalovasilis, P. Partition Geochemistry of Hydrothermal Precipitates from Submarine Hydrothermal Fields in the Hellenic Volcanic Island Arc. *Geochem. Int.* **2014**, *52*, 992–1010. [CrossRef]
33. Liakopoulos, A.; Glasby, G.P.; Papavassiliou, K.; Boulegue, J. Nature and origin of the Vani manganese deposit, Milos, Greece: An overview. *Ore Geol. Rev.* **2001**, *18*, 181–209. [CrossRef]
34. Decher, A.; Bechtel, A.; Echle, W.; Friedrich, G.; Hoernes, S. Stable isotope geochemistry of bentonites from the island of Milos (Greece). *Chem. Geol.* **1996**, *129*, 101–113. [CrossRef]
35. Christidis, G.E.; Huff, W.D. Geological aspects and genesis of bentonites. *Elements* **2009**, *5*, 93–98. [CrossRef]
36. Christidis, G.E. Geochemical correlation of bentonites from Milos Island, Aegean, Greece. *Clay Miner.* **2001**, *36*, 295–306. [CrossRef]
37. Caballero, E.; Reyes, E.; Delgado, A.; Huertas, F.; Linares, J. The formation of bentonite: Mass balance effects. *Appl. Clay Sci.* **1992**, *6*, 265–276. [CrossRef]
38. Schlitzer, R. Ocean Data View. Available online: https://odv.awi.de (accessed on 8 January 2025).
39. Wombacher, F.; Eisenhauer, A.; Heuser, A.; Weyer, S. Separation of Mg, Ca and Fe from geological reference materials for stable isotope ratio analyses by MC-ICP-MS and double-spike TIMS. *J. Anal. At. Spectrom.* **2009**, *24*, 627–636. [CrossRef]
40. Galy, A.; Yoffe, O.; Janney, P.E.; Williams, R.W.; Cloquet, C.; Alard, O.; Halicz, L.; Wadhwa, M.; Hutcheon, I.D.; Ramon, E.; et al. Magnesium isotope heterogeneity of the isotopic standard SRM980 and new reference materials for magnesium-isotope-ratio measurements. *J. Anal. At. Spectrom.* **2003**, *18*, 1352–1356. [CrossRef]
41. Davis, A.M.; Richter, F.M.; Mendybaev, R.A.; Janney, P.E.; Wadhwa, M.; McKeegan, K.D. Isotopic mass fractionation laws for magnesium and their effects on 26Al–26Mg systematics in solar system materials. *Geochim. Cosmochim. Acta* **2015**, *158*, 245–261. [CrossRef]
42. Kleint, C.; Bach, W.; Diehl, A.; Fröhberg, N.; Garbe-Schönberg, D.; Hartmann, J.F.; Koschinsky, A. Geochemical Characterization of Highly Diverse Hydrothermal Fluids from Volcanic Vent Systems of the Kermadec Intra-Oceanic Arc. *Chem. Geol.* **2019**, *528*, 119289. [CrossRef]
43. Price, R.E.; LaRowe, D.E.; Italiano, F.; Savov, I.; Pichler, T.; Amend, J.P. Subsurface Hydrothermal Processes and the Bioenergetics of Chemolithoautotrophy at the Shallow-Sea Vents off Panarea Island (Italy). *Chem. Geol.* **2015**, *407–408*, 21–45. [CrossRef]
44. Price, R.E.; Giovannelli, D. A Review of the Geochemistry and Microbiology of Marine Shallow-Water Hydrothermal Vents. In *Reference Module in Earth Systems and Environmental Sciences*; Elsevier: Amsterdam, Netherlands, 2017; pp. 1–16.
45. Fournier, R.O.; Truesdell, A.H. An empirical Na-K-Ca geothermometer for natural waters. *Geochim. Cosmochim. Acta* **1973**, *37*, 1255–1275. [CrossRef]
46. Ferguson, J.E.; Henderson, G.M.; Kucera, M.; Rickaby, R.E.M. Systematic change of foraminiferal Mg/Ca ratios across a strong salinity gradient. *Earth Planet. Sci. Lett.* **2008**, *265*, 153–166. [CrossRef]
47. Nessim, R.B.; Tadros, H.R.Z.; Abou Taleb, A.E.A.; Moawad, M.N. Chemistry of the Egyptian Mediterranean coastal waters. *Egypt. J. Aquat. Res.* **2015**, *41*, 1–10. [CrossRef]
48. Valsami-Jones, E.; Baltatzis, E.; Bailey, E.H.; Boyce, A.J.; Alexander, J.L.; Magganas, A.; Anderson, L.; Waldron, S.; Ragnarsdottir, K.V. The geochemistry of fluids from an active shallow submarine hydrothermal system: Milos island, Hellenic Volcanic Arc. *J. Volcanol. Geotherm. Res.* **2005**, *148*, 130–151. [CrossRef]

49. Varnavas, S.P.; Cronan, D.S. Submarine hydrothermal activity off Santorini and Milos in the Central Hellenic Volcanic Arc: A synthesis. *Chem. Geol.* **2005**, *224*, 40–54. [CrossRef]
50. Wilckens, F.K.; Reeves, E.P.; Bach, W.; Seewald, J.S.; Kasemann, S.A. Application of B, Mg, Li, and Sr Isotopes in Acid-Sulfate Vent Fluids and Volcanic Rocks as Tracers for Fluid-Rock Interaction in Back-Arc Hydrothermal Systems. *Geochem. Geophys. Geosyst.* **2019**, *20*, 5849–5866. [CrossRef]
51. Teng, F.-Z.; Hu, Y.; Chauvel, C. Magnesium Isotope Geochemistry in Arc Volcanism. *Proc. Natl. Acad. Sci. USA* **2016**, *113*, 7082–7087. [CrossRef]
52. Bischoff, J.L.; Dickson, F.W. Seawater-Basalt Interaction at 200 °C and 500 Bars: Implications for Origin of Sea-Floor Heavy-Metal Deposits and Regulation of Seawater Chemistry. *Earth Planet. Sci. Lett.* **1975**, *25*, 385–397. [CrossRef]
53. Pichler, T.; Veizer, J.; Hall, G.E. The Chemical Composition of Shallow-Water Hydrothermal Fluids in Tutum Bay, Ambitle Island, Papua New Guinea, and Their Effect on Ambient Seawater. *Mar. Chem.* **1999**, *64*, 229–252. [CrossRef]
54. Parkhurst, D.L.; Appelo, C. *Description of Input and Examples for PHREEQC Version 3: A Computer Program for Speciation, Batch-Reaction, One-Dimensional Transport, and Inverse Geochemical Calculations*; U.S. Geological Survey: Reston, VA, USA, 2013; pp. 1–497.
55. Sætre, C.; Hellevang, H.; Riu, L.; Dypvik, H.; Pilorget, C.; Poulet, F.; Werner, S.C. Experimental Hydrothermal Alteration of Basaltic Glass with Relevance to Mars. *Meteorit. Planet. Sci.* **2019**, *54*, 357–378. [CrossRef]
56. Hall, D.M.; Lvov, S.N.; Gamwo, I.K. Thermodynamic Modeling of Mineral Scaling in High-Temperature and High-Pressure Aqueous Environments. *Liquids* **2022**, *2*, 303–317. [CrossRef]
57. Tivey, M.K. Generation of Seafloor Hydrothermal Vent Fluids and Associated Mineral Deposits. *Oceanography* **2007**, *20*, 50–65. [CrossRef]
58. Liakopoulos, A.; Katerinopoulos, A.; Markopoulos, T.; Boulegue, J. A Mineralogical, Petrographic, and Geochemical Study of Samples from Wells in the Geothermal Field of Milos Island (Greece). *Geothermics* **1991**, *20*, 237–256. [CrossRef]
59. Teng, F.-Z.; Li, W.-Y.; Ke, S.; Marty, B.; Dauphas, N.; Huang, S.; Wu, F.-Y.; Pourmand, A. Magnesium Isotopic Composition of the Earth and Chondrites. *Geochim. Cosmochim. Acta* **2010**, *74*, 4150–4166. [CrossRef]
60. Fytikas, M. Updating of the Geological and Geothermal Research on Milos Island. *Geothermics* **1989**, *18*, 485–496. [CrossRef]
61. Tipper, E.T.; Galy, A.; Bickle, M.J. Riverine Evidence for a Fractionated Reservoir of Ca and Mg on the Continents: Implications for the Oceanic Ca Cycle. *Earth Planet. Sci. Lett.* **2006**, *247*, 267–279. [CrossRef]
62. Hu, Z.; Li, W.; Hohl, S.V.; Meister, P.; Yang, S.; Zhang, B.; Xia, Z.; Liu, C. Evaporite Sequences as Archives for Mg Isotope Compositions of Seawater—Evidence from a Tethys Marginal Shelf Basin in the Anisian. *Chem. Geol.* **2024**, *668*, 122346. [CrossRef]
63. Eom, J.; Yoshimura, T.; Araoka, D.; Gamo, T.; Kawahata, H. Magnesium Isotopic Composition of Submarine Vent Fluids from Arc and Back-Arc Hydrothermal Systems in the Western Pacific. *Chem. Geol.* **2020**, *551*, 119767. [CrossRef]
64. Pogge von Strandmann, P.A.; Burton, K.W.; Opfergelt, S.; Eiríksdóttir, E.S.; Murphy, M.J.; Einarsson, A.; Gislason, S.R. Hydrothermal and Cold Spring Water and Primary Productivity Effects on Magnesium Isotopes: Lake Myvatn, Iceland. *Front. Earth Sci.* **2020**, *8*, 109. [CrossRef]
65. Leeman, W.P.; Tonarini, S.; Pennisi, M.; Ferrara, G. Boron Isotopic Variations in Fumarolic Condensates and Thermal Waters from Vulcano Island, Italy: Implications for Evolution of Volcanic Fluids. *Geochim. Cosmochim. Acta* **2005**, *69*, 143–163. [CrossRef]
66. Daskalopoulou, K.; Gagliano, A.L.; Calabrese, S.; Longo, M.; Hantzis, K.; Kyriakopoulos, K.; D'Alessandro, W. Gas Geochemistry and CO2 Output Estimation at the Island of Milos, Greece. *J. Volcanol. Geotherm. Res.* **2018**, *365*, 13–22. [CrossRef]
67. Kakihana, H.; Kotaka, M.; Satoh, S.; Nomura, M.; Okamoto, M. Fundamental Studies on the Ion-Exchange Separation of Boron Isotopes. *Bull. Chem. Soc. Jpn.* **1977**, *50*, 158–163. [CrossRef]
68. Hershey, J.P.; Fernandez, M.; Milne, P.J.; Millero, F.J. The Ionization of Boric Acid in NaCl, Na-Ca-Cl, and Na-Mg-Cl Solutions at 25 °C. *Geochim. Cosmochim. Acta* **1986**, *50*, 143–148. [CrossRef]
69. Spivack, A.J.; Edmond, J.M. Boron Isotope Exchange Between Seawater and the Oceanic Crust. *Geochim. Cosmochim. Acta* **1987**, *51*, 1033–1043. [CrossRef]

Disclaimer/Publisher's Note: The statements, opinions and data contained in all publications are solely those of the individual author(s) and contributor(s) and not of MDPI and/or the editor(s). MDPI and/or the editor(s) disclaim responsibility for any injury to people or property resulting from any ideas, methods, instructions or products referred to in the content.